Magn Reson Mater Phy (2014) 27:185–193
DOI 10.1007/s10334-013-0400-9

RESEARCH ARTICLE

Quantitative breast MRI: 2D histogram analysis of diffusion tensor parameters in normal tissue

Julia Wiederer · Shila Pazahr · Cornelia Leo · Daniel Nanz · Andreas Boss

Received: 11 April 2013 / Revised: 12 July 2013 / Accepted: 19 August 2013 / Published online: 3 September 2013

Abstract
Object Diffusion tensor imaging (DTI) of the breast may provide a powerful new approach for the detection of intraductal processes. The aim of this investigation was to characterize the relation between diffusion tensor parameters [fractional anisotropy (FA), mean diffusivity (MD)] in normal breast tissue to obtain information on the microenvironment of the diffusing water molecules and to provide a systematic approach for DTI analysis.
Materials and methods Seven female, healthy volunteers underwent prospective double-spin-echo prepared echo-planar diffusion-weighted sequence (TR/TE 8,250 ms/74 ms, *b* values 0 and 500 s/mm (2), six encoding directions, 12 averages, 35 slices) in 4 consecutive weeks (3.0 T). Quantitative maps of diffusion tensor parameters were computed offline with custom routines. The interdependence of MD and FA in different voxels was analysed by linear and exponential regression.
Results All MD and FA maps were of excellent quality. A consistent pattern was observed in that lower fractional anisotropy values were more likely associated with higher mean diffusivity values. The dependence exhibited an exponential behavior with a correlation coefficient $R = 0.60$ (R linear $= 0.57$).
Conclusion The likelihood with which FA and MD values are observed in a voxel within normal breast tissue is characterized by a specific pattern, which can be described by an exponential model. Moreover, we could show that the proposed technique does not depend on the menstrual cycle.

Keywords Breast MRI · DTI · Menstrual cycle

J. Wiederer (✉) · S. Pazahr · D. Nanz · A. Boss
Institute of Diagnostic and Interventional Radiology, University Hospital of Zurich, Raemistr. 100, 8091 Zurich, Switzerland
e-mail: julia.wiederer@usz.ch

C. Leo
Division of Gynecology, University Hospital of Zurich, Zurich, Switzerland

Introduction

Contrast enhanced MRI (CE-MRI) is a widely used modality in breast imaging and the most sensitive method in detecting invasive breast cancer particularly in mammographically heterogeneous dense and very dense breasts. However, the assessment of CE-MRI examinations can be challenging for small intraductal processes such as ductal carcinoma in situ (DCIS) [1–3].

Ductal carcinoma in situ constitutes a heterogeneous entity of abnormal epithelial cell proliferation within the duct network that is still limited by the basement membrane. A variable percentage of progression to invasive cancerous disease has been reported [4, 5]. Although CE-MRI is superior to mammography in detecting DCIS and can demonstrate the true extent of DCIS more accurately, it is still not possible to predict DCIS subtypes or definitely discriminate the more aggressive high grade form from low grade or intermediate grade DCIS [6]. The increasing performance of screening mammography raises the number of non-palpable suspicious breast lesions and 20 % of screening-detected malignancies represent DCIS [7, 8].

Diffusion-weighted imaging (DWI) is established in neuroimaging for assessment of cerebral infarction and tumor characterization. Within the last few years further interest has been focused on the detection of malignancies using whole-body DWI [9, 10]. Initial applications of DWI in breast tissue in recent investigations suggest a potential

to improve differentiation of benign from malignant mass-like lesions [11]. Rahbar et al. [12] reported lower ADC values in "pure" DCIS lesions than in normal breast tissue, which may be due to increased degree of cellularity.

The architecture of breast tissue is complex and comprises a compound of tubular and ligamentous structures, such as the duct network, terminal ductal lobular units, and periductal stroma components. Because of anisotropic water diffusion in the small ducts, diffusion tensor imaging (DTI) may provide a powerful new approach to obtain information on physiological and pathological changes of breast-tissue architecture.

The inhomogeneity of breast tissue can easily cause large inter-reader variations via small differences in the definition of the region-of-interest (ROI). The main topic of our study was to define and test a methodology for a systematic analysis of diffusion tensor parametrical maps of breast parenchyma that may less strongly depend on exact ROI positioning by using a 2D histogram analysis of the interdependence of mean diffusivity and fractional anisotropy values. The proposed technique of DTI imaging and post-processing has been applied in a cohort of healthy young women at four different time points during the menstrual cycle (1) to obtain baseline information on diffusion tensor data, and (2) to investigate cycle-dependent variability in DTI measurements. Furthermore, (3) the clinical applicability of the proposed method has been tested in two patients.

Materials and methods

Subjects

Volunteers

After approval by the local ethics committee, seven healthy, premenopausal, female volunteers (age between 24 and 41 years, mean age 32.3 ± 5.1 years) agreed to the examination and were included in the study. They all had regular, approximately 28-day, menstrual cycles during a minimum of the last 6 months. None of the volunteers were taking oral contraceptives or had an intra-uterine device. None of them had a history of breast disease, breast biopsy or breast operation and all were nulliparous.

In each of 4 consecutive weeks one MRI exam was conducted. No specific preparations were undertaken prior to any examination. The week of the menstrual cycle for each scan was determined by the reported menstruation dates.

Week 1 started on the first day of menstruation.

- Week 1: Day 1–7 of cyclus.
- Week 2: Day 8–14.
- Week 3: Day 15–21.
- Week 4: Day 22–28.

Patients

Two patients were included undergoing clinically indicated breast MRI (diagnoses: invasive-ductal carcinoma and chronic granulating inflammation). Both patients agreed to the acquisition of the additional DTI sequence, which was included into the clinical protocol before contrast-media application.

Imaging protocol

All volunteer data were acquired on a 3.0 T whole-body MR scanner (Discovery MR 750, GE Healthcare, Waukesha, MI, USA) using a dedicated breast-coil of the same manufacturer.

After a gradient-echo localizer, a morphological T2w fast spin echo sequence (TR 10,766 ms, TE 100.3 ms, fast spin echo factor 21, matrix 512 × 512, in-plane resolution 0.7 × 0.7 mm^2, slice thickness 3 mm) was acquired in axial orientation.

Diffusion tensor images were acquired in axial orientation with a fat-saturated double-spin-echo prepared echo-planar imaging sequence (TR 8,250 ms, TE 75 ms, bandwidth 1953 Hz/px, matrix size 256 × 128, *b* value 500 s/mm^2, in-plane resolution 1.36 × 1.36 mm^2, slice thickness 4 mm, 12 averages, parallel imaging factor 2). The diffusion-sensitizing gradient fields were applied in 6 directions.

The patient examinations were carried out in a different 3.0 T whole-body scanner (Siemens Skyra, Erlangen, Germany) with a dedicated breast-coil. The DTI sequence was a fat-saturated double-spin-echo echo-planar imaging sequence (TR 5,300 ms, TE 57 ms, bandwidth 1,490 Hz/px, matrix size 210 × 96, *b* value 500 s/mm^2, in-plane resolution 1.71 × 1.71 mm^2, slice thickness 4 mm, parallel imaging factor 2). The clinical imaging protocol also included an axial 2D T2-weighted fast spin-echo sequence and repeated acquisitions with a 3D dynamic gradient-echo sequence.

Post processing

The averaged diffusion-weighted images were analysed using adapted routines written in Matlab (The Mathworks, Inc., Natick, MA, USA). The diffusion tensor elements were evaluated as reported by Basser [13] on a pixel-by-pixel basis. After calculation of the diffusion tensor, the tensor was diagonalized and parametrical maps were calculated starting from the computed principal diffusivity

components, D_1, D_2, and D_3. The fractional anisotropy is defined as

$$\mathrm{FA} = \frac{\sqrt{3\left((D_1 - \mathrm{MD})^2 + (D_2 - \mathrm{MD})^2 + (D_3 - \mathrm{MD})^2\right)}}{\sqrt{2\left(D_1^2 + D_2^2 + D_3^2\right)}}$$

with the mean diffusivity being defined as

$$\mathrm{MD} = \frac{D_1 + D_2 + D_3}{3}.$$

The fractional anisotropy is a quantitative measure for the "average orientedness" of the diffusion-hindering microstructures in a voxel. If those structures allowed diffusion only along a single direction, a maximum FA value of 1 is expected, whereas completely free or isotropically restricted diffusion should result in a FA of 0. The MD is a measure for the overall presence of obstacles to diffusion. A high MD can be computed in water-like fluid, in which free diffusion occurs.

Regions-of-interest were defined on the parametrical maps comprising all of the breast tissue on one side on the respective slice. A typical example is provided in Fig. 1. In the ROI, all voxels with MD $< 0.1 \times 10^{-3}$ mm^2/s (corresponding to fatty tissue) were omitted from the evaluation.

The correlation between MD and FA values observed in the remaining voxels within the ROI was explored with two different models, which are the most elementary models to describe the MD-FA interdependence:

1. A linear least-squares fit with computation of a slope m for a linear model:

$$\mathrm{FA}(\mathrm{MD}) = m \cdot \mathrm{MD} + \mathrm{FA}(0)$$

2. A non-linear least-squares fit based on the Levenberg–Marquardt Algorithm was applied to the following expression.

$$\mathrm{FA}(\mathrm{MD}) = \mathrm{FA}(0) \cdot e^{-\frac{\mathrm{MD}}{k}}$$

with computation of k for an exponential model.

Correlation coefficients R_{lin} and R_{exp} were calculated between the measured FA values of each voxel and the calculated ("predicted") FA values using the measured MD value of the voxel in the linear or exponential model and the corresponding fitting parameters.

Mean values and standard deviations were computed for m, k, R_{lin}, and R_{exp} in the left and right breast for each of the four MR exams of each volunteer.

Furthermore, MD pixel values were subdivided into two groups: group A ("low") with MD values $<1.5 \times 10^{-3}$ mm^2/s, and group B ("high") with MD values $>1.5 \times 10^{-3}$ mm^2/s. From both groups, mean values and standard deviations of MD and FA ($\mathrm{MD_{low}}$, $\mathrm{MD_{high}}$, $\mathrm{FA_{low}}$, $\mathrm{FA_{high}}$) were computed and averaged again for the cohort of volunteers.

In the two patients, pathological tissue identified in the contrast-enhanced sequences was analyzed with the above described post-processing steps and compared to healthy breast tissue from the same patient in the contralateral breast.

Values of m, k, R_{lin}, R_{exp}, $\mathrm{MD_{low}}$, $\mathrm{MD_{high}}$, $\mathrm{FA_{low}}$, $\mathrm{FA_{high}}$ observed in week 2 of the menstrual cycle were tested for statistically significant differences versus measurements of week 1, 3, and 4 using a paired two-sided Students' t test. The same test was applied to check for right and left side differences. Finally, the correlation coefficients R_{lin} and R_{exp} and the fractional anisotropies $\mathrm{FA_{low}}$ and $\mathrm{FA_{high}}$ were tested for significant differences using the paired two-sided Students' t test. p values below 0.05 were considered statistically significant.

Results

All volunteers and patients, respectively, tolerated the four single examinations well. In none of the diffusion-tensor data sets could relevant movement artifacts be identified. Exemplary MD and FA parametrical maps are shown in Fig. 2. In all volunteers the highest MD values were found in the central areas of the breast parenchyma, which are

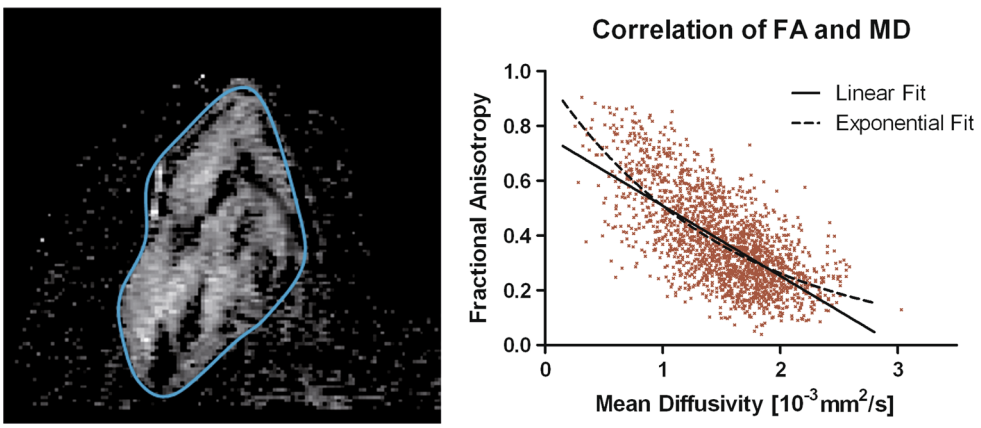

Fig. 1 Example of a region-of-interest (ROI) placed on a mean diffusivity map comprising the whole- breast parenchyma on one side. To the right, the corresponding MD–FA diagram is displayed with a linear and exponential fit, respectively

directed towards the breast papilla. Towards the periphery of the breast parenchyma, a decline of the MD was seen. The central areas of high MD corresponded to areas of low FA, whereas the peripheral areas of low MD showed relatively high FA.

A graphical representation of these findings is displayed on the right side of Fig. 1 in the form of an "MD–FA" diagram. A decline is seen from the upper left part of the diagram towards the lower right part. For a quantitative mathematical summary of the behavior, the points in the MD–FA plot were fitted to linear and exponential models. The results are summarized in Table 1. For none of the evaluated parameters was a statistically significant difference found comparing the measurements of weeks 1–4 or comparing the right to the left side. Therefore, the mean values of all four measurements, displayed on the right side of Table 1, were used for the further evaluations.

The exponential model approximated the dependence between MD and FA slightly better with a higher absolute value of the correlation coefficient ($R_{exp} = 0.55 \pm 0.14$ vs. $R_{lin} = 0.52 \pm 0.15$, $p < 0.001$). The mean FA for voxels with MD smaller than 1.5×10^{-3} mm^2/s was higher ($FA_{low} = 0.48 \pm 0.06$) than the mean FA of voxels with MD higher than 1.5×10^{-3} mm^2/s ($FA_{high} = 0.28 \pm 0.09$, $p < 0.001$).

When applying the proposed evaluation technique to two patients with non-masslike breast lesions, notable differences from these typical patterns were observed (Figs. 3, 4). The parametrical values of both patients are reported in Table 2. In the patient with invasive-ductal carcinoma, a shift of the diffusion values towards higher MD can be noted: 20.9 % of the voxels were in the MD_{low} group, compared to 66.9 % in healthy parenchyma of the same patient (69.0 % in the group of healthy volunteers). The voxels in the MD_{low} group also showed lower FA values with 0.29 ± 0.09 versus 0.18 ± 0.13 in the healthy tissue. Correspondingly, the curve in the MD–FA diagram was more flat, with smaller absolute values of m and k compared to the healthy contralateral tissue: $m = -0.10$ versus -0.19×10^3 s/mm^2 in the linear fit, and $k = 1.54$ versus 1.66×10^{-3} mm^2/s in the exponential fit.

In the patient with chronic inflammation, a steeper curve was seen in the MD–FA diagram on the affected side compared to healthy breast tissue with an increased absolute value of the slope $m = -0.22$ versus -0.16×10^3 s/mm^2 and a higher constant $k = 1.46$ versus 1.34×10^{-3} mm^2/s. Also, more voxels were shifted towards lower MD and higher FA values in the ROI of chronic inflammation with 94.4 % of the voxels in the MD_{low} group ($FA = 0.37 \pm 0.16$) compared to the contralateral ROI in healthy tissue with 35.6 % of the voxels in the MD_{low} group, ($FA\ 0.28 \pm 0.13$) (Table 3).

Discussion

In the presented study, we investigated statistical relations between the DTI parameters MD and FA within healthy breast tissue. We found a typical pattern with central areas of relatively high MD and low FA values surrounded by tissue of lower MD with markedly increased FA values. MD–FA diagrams provided a visualization of the statistical relation of the two diffusion parameters, which was better reflected with a two-parameter exponential model than

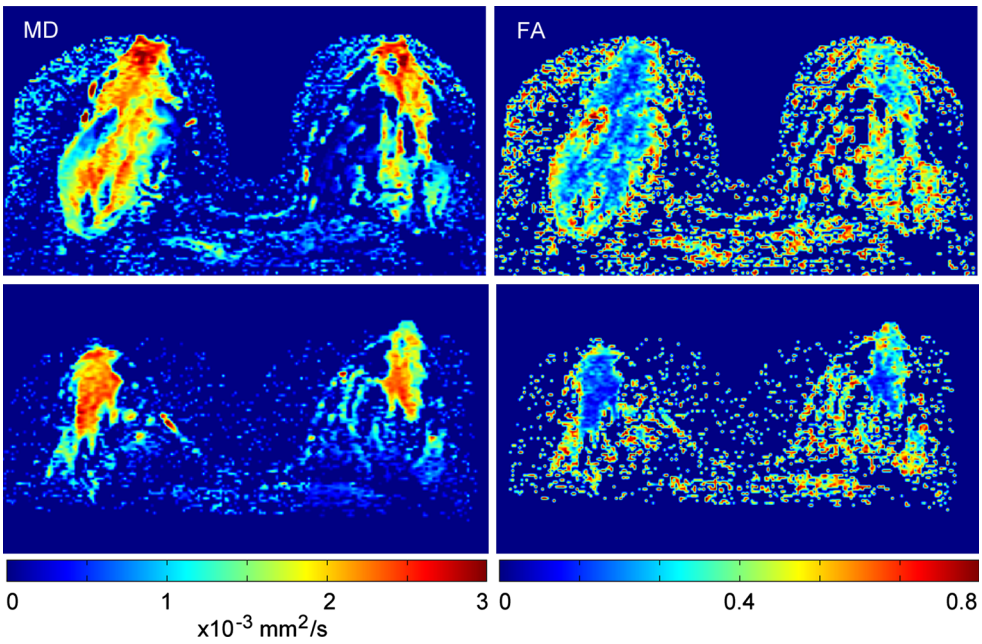

Fig. 2 Colour-encoded mean diffusivity and fractional anisotropy parametrical maps in two healthy volunteers (*top* and *bottom row*, respectively) are displayed. In the central areas of strong diffusion indicated by *orange to red colour* on the *left side*, the respective fractional anisotropy is small (*blue colour*), whereas in the marginal areas intermediate to strong diffusion anisotropy can be noted (*green to red colour*)

Table 1 Diffusion tensor and fitting parameters for healthy volunteers

	Right breast				Left breast				Mean
	Week 1	Week 2	Week 3	Week 4	Week 1	Week 2	Week 3	Week 4	
m	0.19 ± 0.06	0.21 ± 0.05	0.10 ± 0.16	0.17 ± 0.05	0.18 ± 0.06	0.22 ± 0.05	0.19 ± 0.06	0.18 ± 0.05	0.18 ± 0.08
R_{lin}	0.57 ± 0.13	0.58 ± 0.13	0.47 ± 0.20	0.50 ± 0.15	0.48 ± 0.19	0.58 ± 0.09	0.50 ± 0.15	0.53 ± 0.09	0.52 ± 0.15
k	1.90 ± 0.63	1.62 ± 0.86	2.61 ± 2.08	1.90 ± 0.52	2.20 ± 1.28	1.63 ± 0.88	1.77 ± 0.50	1.57 ± 0.46	1.91 ± 1.10
R_{exp}	0.60 ± 0.11	0.60 ± 0.13	0.49 ± 0.20	0.54 ± 0.14	0.51 ± 0.18	0.60 ± 0.08	0.54 ± 0.13	0.56 ± 0.10	0.55 ± 0.14
MD_{low}	1.15 ± 0.14	1.19 ± 0.06	1.18 ± 0.10	1.20 ± 0.05	1.12 ± 0.13	1.18 ± 0.09	1.15 ± 0.11	1.16 ± 0.10	1.16 ± 0.10
FA_{low}	0.49 ± 0.09	0.44 ± 0.03	0.48 ± 0.06	0.50 ± 0.05	0.49 ± 0.06	0.48 ± 0.05	0.50 ± 0.06	0.44 ± 0.07	0.48 ± 0.06
MD_{high}	2.02 ± 0.18	1.98 ± 0.11	1.99 ± 0.15	2.07 ± 0.14	1.97 ± 0.13	2.01 ± 0.12	1.95 ± 0.15	2.02 ± 0.19	2.0 ± 0.15
FA_{high}	0.30 ± 0.09	0.26 ± 0.07	0.31 ± 0.06	0.29 ± 0.05	0.32 ± 0.15	0.27 ± 0.08	0.30 ± 0.06	0.24 ± 0.07	0.28 ± 0.09
N_{low}	35.9 ± 25.0	31.6 ± 22.4	36.0 ± 24.9	19.0 ± 9.3	40.5 ± 32.6	26.5 ± 17.6	38.8 ± 27.6	28.1 ± 26.5	32.2 ± 25.2

m: Absolute value of slope of linear regression (in 10^3 s/mm^2)

R_{lin}: Correlation coefficient of linear regression

k: Characteristic constant of exponential fit (in 10^{-3} mm^2/s)

R_{exp}: Correlation coefficient of exponential fit

MD_{low}: Mean MD of voxels with MD $\leq 1.5 \times 10^{-3}$ mm^2/s (in 10^{-3} mm^2/s)

FA_{low}: Mean FA of voxels with MD $\leq 1.5 \times 10^{-3}$ mm^2/s

MD_{high}: Mean MD of voxels with MD $> 1.5 \times 10^{-3}$ mm^2/s (in 10^{-3} mm^2/s)

FA_{high}: Mean FA of voxels with MD $> 1.5 \times 10^{-3}$ mm^2/s

N_{low}: Percentage of voxels with MD $\leq 1.5 \times 10^{-3}$ mm^2/s (%)

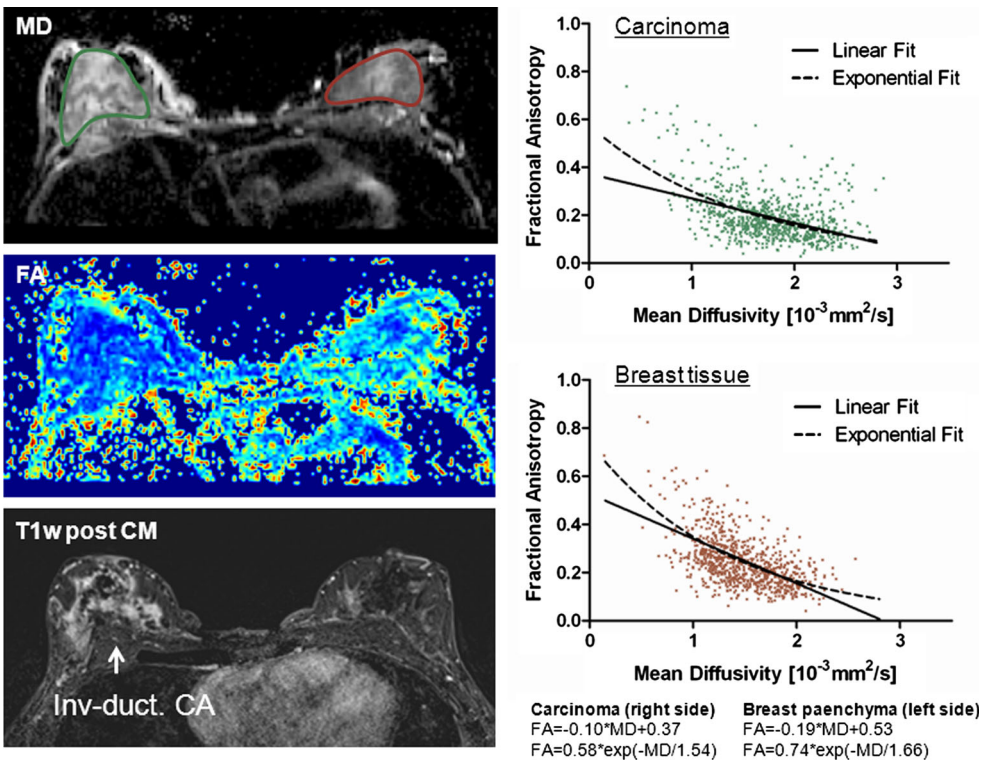

Fig. 3 Images of a 45 year-old patient with invasive-ductal breast cancer on the right side. Mean diffusivity, fractional anisotropy and post-contrast T1w images are shown on the *left*. In the breast cancer, higher diffusion can be seen with lower fractional anisotropy compared on the healthy left side. Correspondingly, in the MF–FA diagram, flatter curves are obtained in the linear regression (slope m −0.10 vs. -0.19×10^3 s/mm^2) and the exponential fitting (characteristic constant k 1.54 vs. 1.33 $\times$ 10^{-3} s/mm^2)

with a two-parameter linear model. To our knowledge, this is the first study describing this typical statistical distribution pattern of diffusion parameters in breast tissue. Furthermore, we found preliminary evidence that while this pattern and the corresponding fit parameters were relatively stable across different phases of the menstrual cycle and across individuals it may be significantly altered in diffuse breast disease, such as breast cancer or inflammation.

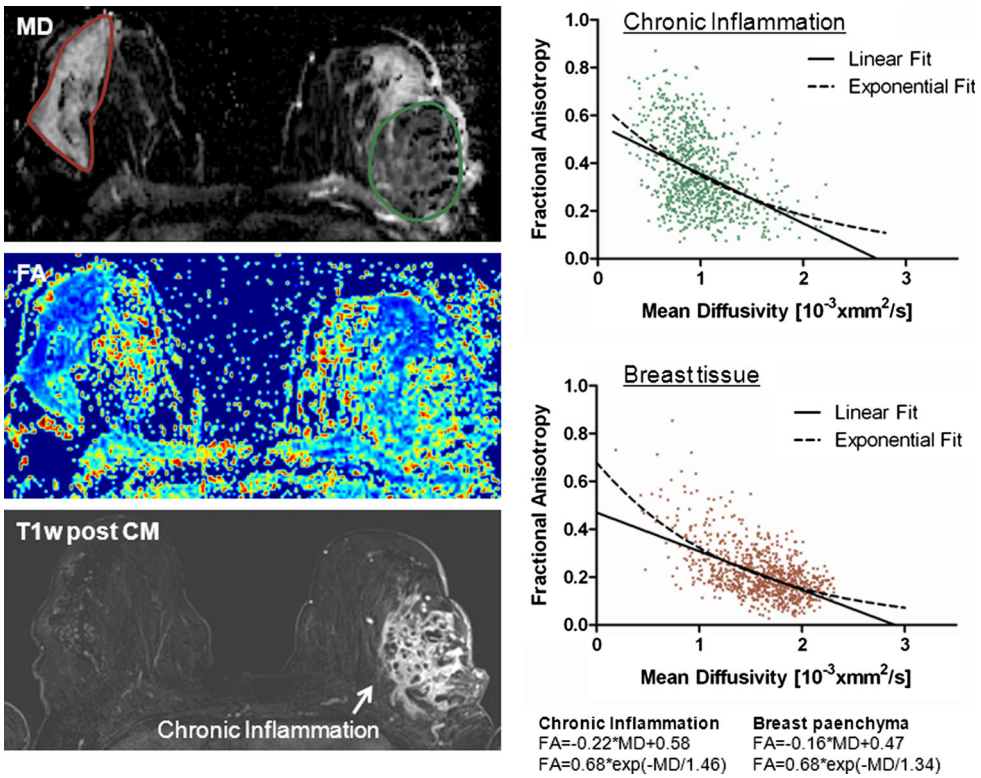

Fig. 4 A 34 year-old patient with chronic granulomatous inflammation in the left side. Mean diffusivity, fractional anisotropy maps, and post-contrast T1w images are displayed on the *left*. In the MD map, the region-of-interest measurements are indicated in *dark red* and *green* colour. The area of chronic inflammation exhibits a diffusion restriction with markedly increased fractional anisotropy. Correspondingly, a steeper decrease of the fit can be seen in the MD-FA diagram compared to healthy breast tissue with a higher absolute value of the slope m of the linear regression (-0.22 vs. -0.16×10^3 s/mm^2) and a higher characteristic constant k in the exponential fit (1.46 vs. 1.34×10^{-3} s/mm^2)

Table 2 p Values for comparison of diffusion tensor and fitting parameters at weeks 1, 3, and 4 to the values from week 2 for healthy volunteers

	Right breast			Left breast		
	Week 1	Week 3	Week 4	Week 1	Week 3	Week 4
m	0.78	0.08	0.41	0.08	0.45	0.07
R_{lin}	0.86	0.07	0.67	0.22	0.24	0.28
k	0.40	0.12	0.69	0.19	0.77	0.82
R_{exp}	0.89	0.08	0.77	0.24	0.30	0.40
MD_{low}	0.55	0.98	0.74	0.40	0.75	0.94
FA_{low}	0.32	0.20	0.09	0.85	0.67	0.19
MD_{high}	0.93	0.82	0.07	0.82	0.49	0.20
FA_{high}	0.09	0.06	0.19	0.60	0.55	0.09
N_{low}	0.07	0.25	0.06	0.35	0.24	0.64

Diffusion tensor imaging parameters reflect averaged tissue microstructure in the breast. A typical histological hematoxylin–eosin stained histological image of normal breast parenchyma is provided in Fig. 5. The diameter of the normal milk ducts is on the order of 0.1 mm which can increase even in the non-lactating breast 10–20 times by the accumulation of fluid [14]. It may be hypothesized that the high FA values in the periphery reflect the terminal ductal lobular units or very small peripheral ducts with slower water diffusion and a higher anisotropy. In contrast, high MD in the central parts could illustrate the major ducts directed towards the nipple with a lower anisotropy. The lower anisotropy of the water diffusion in the major ducts in spite of their directionality towards the nipple may be attributed to the larger diameter of these ducts, which maybe sufficiently large to not significantly hinder the Brownian motion of the water molecules.

The potential influence of the ligamentous structures and their regional distribution differences on DTI parameters should also be considered [15]. It seems interesting to compare our data from non-lactating women with measurements in lactating breasts to see if there is a notable difference in anisotropy and to identify the anatomic correlate of anisotropy in the breast. In early pregnancy, breast tissue is already stimulated by increasing oestrogen levels [16]. Therefore, breast volume increases, histologically mainly corresponding to the development of the ductal network. Assuming that the ductal system is collapsed in non-lactating women we would expect changes in fractional anisotropy if applying DTI measurements in lactating women. This could support our theory that the ductal network is the main anatomical correlate in the breast and that regional differences of fractional anisotropy are caused by different sizes of milk ducts.

Regional differences in ADC and FA were previously described by Partridge et al. [17]. In a study with 12 healthy women, ADC and FA were significantly affected by location in the breast. ROI-analysis was performed in the anterior, posterior and central parts of the breast.

Although the definition of the regions was subjective and the ROIs were small, Partridge et al. could show a significantly higher ADC in central parts of the breast than in the posterior breast which is concordant to our data. Also, regional differences in FA were demonstrated with significantly higher FA in the posterior parts than in the anterior and central breast. Moreover, our results are in accordance with a study of Baltzer et al. [18] reporting that the main diffusion direction is anterior-posterior. The published broad range of ADC (0.89–1.67 $\times$ 10^{-3} mm^2/s) and FA (0.20–0.41) values is consistent with our observations. Furthermore, our mean diffusivity values and the distribution pattern of fractional anisotropy within the breast are consistent with data reported from Eyal et al. [19].

Table 3 Diffusion tensor and fitting parameters for the two patients

	Patient 1		Patient 2	
	Normal tissue	Inv.-duct. cancer	Normal tissue	Inflammation
m	0.19	0.10	0.16	0.22
R_{lin}	0.49	0.45	0.56	0.42
k	1.66	1.54	1.34	1.46
R_{exp}	0.53	0.52	0.59	0.45
MD_{low}	1.25 ± 0.16	1.32 ± 0.20	1.19 ± 0.25	0.92 ± 0.24
FA_{low}	0.29 ± 0.09	0.18 ± 0.13	0.28 ± 0.13	0.37 ± 0.16
MD_{high}	1.80 ± 0.19	1.98 ± 0.30	1.82 ± 0.20	1.80 ± 0.26
FA_{high}	0.21 ± 0.08	0.16 ± 0.07	0.18 ± 0.07	0.24 ± 0.12
N_{low}	66.9	20.9	35.6	94.4

m: Absolute value of slope of linear regression (in 10^3 s/mm^2)

R_{lin}: Absolute value of correlation coefficient of linear regression

k: Characteristic constant of exponential fit (in 10^{-3} mm^2/s)

R_{exp}: Correlation coefficient of exponential fit

MD_{low}: Mean MD of voxels with MD $\leq$ 1.5 $\times$ 10^{-3} mm^2/s (in $10^{-3}mm^2/s$)

FA_{low}: Mean FA of voxels with MD $\leq$ 1.5 $\times$ 10^{-3} mm^2/s

MD_{high}: Mean MD of voxels with MD $>$ 1.5 $\times$ 10^{-3} mm^2/s (in $10^{-3}mm^2/s$)

FA_{high}: Mean FA of voxels with MD $>$ 1.5 $\times$ 10^{-3} mm^2/s

N_{low}: Percentage of voxels with MD $\leq$ 1.5 $\times$ 10^{-3} mm^2/s (%)

In 2001, Partridge et al. [17] published that there is no significant influence of menstrual cycle on breast ADC values and only a trend of decreased ADC during the second week and increased ADC during the fourth week. These early observations were later confirmed by O'Flynn et al. [20]. These observations from DWI are in good agreement with the data from our DTI analysis.

In both of the evaluated patients in our study, a notable change of this physiological diffusion pattern was seen suggesting its suitability for the assessment and characterization of pathological (non-masslike) changes of breast tissue. In contrast to the literature, the patient with the grade 3 invasive ductal carcinoma with associated high grade DCIS (Fig. 3) demonstrated elevated mean diffusivity but lower fractional anisotropy compared to the contralateral breast, whereas in most previous reports a decrease of the mean diffusivity in cancerous tissue was reported. In the case of our patient, the higher mean diffusivity may potentially be caused by the large extent of the tumor infiltration and subsequent small necrosis zones, which, however, were not visible on the contrast-enhanced sequences. An opposite finding was measured in our patient with chronic inflammation of the breast. In this condition duct obliteration due to secretory debris and

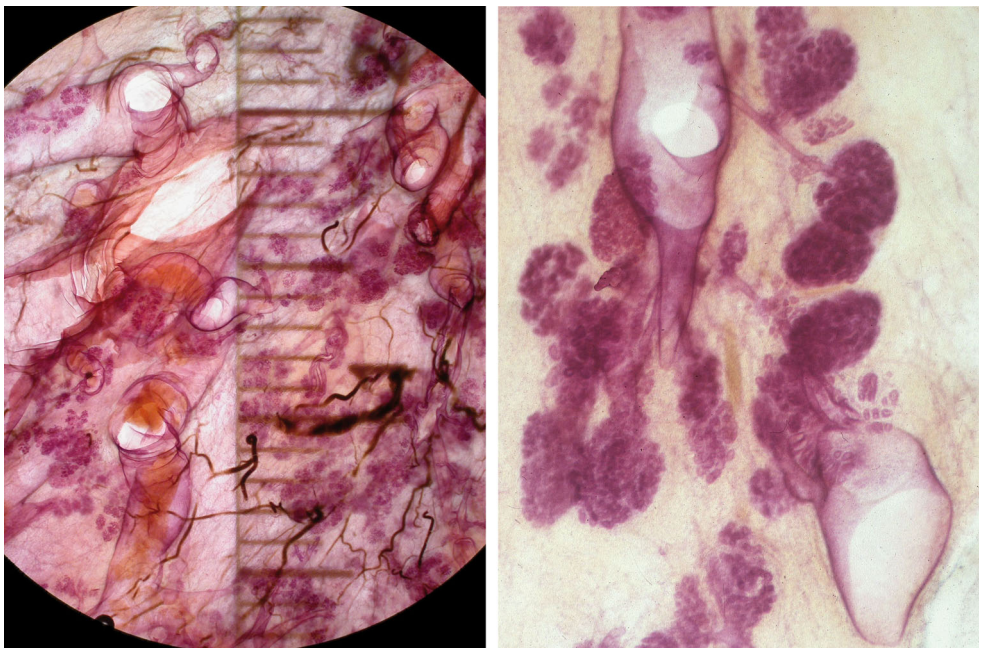

Fig. 5 Histological images (hematoxylin–eosin staining) of breast parenchyma with intermediate magnification (*left side*) and strong magnification (*right side*). The scale on the left side is in millimeters. *Left side* shows normal parenchyma with slightly dilated ducts filled with fluid, *right side* displays several normal terminal ductal lobular units (TDLUs) and largely dilated ducts. Images are provided courtesy of Prof. László Tabár

macrophages can be found. One hypothesis is that due to the lower diffusion within the obliterated ducts, higher diffusion anisotropy is measured which cannot be observed in normal ducts due to the faster water diffusion.

As Tabar showed that neoductgenesis is the anatomical correlate of DCIS [21, 22], one interesting application of our technique would be to apply our analysis of DTI data in patients with pure DCIS in order to obtain data about potential anisotropy in so-called neoducts compared to normal breast tissue. In addition, further studies are planned to focus on the influence of different DCIS subtypes on the DTI pattern. Because of logistical (fast treatment planning) and psychological issues, the preoperative contrast enhanced MRI in premenopausal women with newly diagnosed breast cancer has to be planned in some cases without considering the menstrual cycle, although several studies revealed the influence of the cycle to the background enhancement in CE-MRI [23, 24]. For such an indication, the DTI technique may provide additional important clinical information as it is demonstrated to be highly robust against hormonal influences from the menstrual cycle.

Our study has several limitations. Firstly, only seven healthy volunteers were included in our prospective study but all of them underwent MRI acquisition in 4 consecutive weeks showing only little variability of the DTI parameters. Secondly, only one radiologist (blinded for review) performed the ROI analysis. However, in this study the ROI analysis included the whole-breast parenchyma at a slice through the nipple, which is a highly standardized approach with less reader dependence compared to the choice of some part of the breast tissue. Thirdly, we included only two patients with breast diseases in our study. However, in both patients we detected notable deviations from the otherwise robust physiological diffusion pattern suggesting the potential clinical usefulness of the evaluation scheme.

Conclusion

The probabilistic distribution patterns of DTI parameters in the breast may offer a robust, cycle independent characterization of breast microstructure. MD–FA diagrams can be described with an exponential model, which might react sensitively to the occurrence of pathological alterations.

References

1. Orel SG, Schnall MD (2001) MR imaging of the breast for the detection, diagnosis, and staging of breast cancer. Radiology 220(1):13–30
2. Berg WA, Gutierrez L, NessAiver MS, Carter WB, Bhargavan M, Lewis RS, Ioffe OB (2004) Diagnostic accuracy of mammography, clinical examination, US, and MR imaging in preoperative assessment of breast cancer. Radiology 233(3):830–849
3. Peters NH, Borel Rinkes IH, Zuithoff NP, Mali WP, Moons KG, Peeters PH (2008) Meta-analysis of MR imaging in the diagnosis of breast lesions. Radiology 246(1):116–124
4. Kuhl CK, Schrading S, Bieling HB, Wardelmann E, Leutner CC, Koenig R, Kuhn W, Schild HH (2007) MRI for diagnosis of pure ductal carcinoma in situ: a prospective observational study. Lancet 370(9586):485–492
5. Kuhl CK (2009) Why do purely intraductal cancers enhance on breast MR images? Radiology 253(2):281–283
6. Rahbar H, Partridge SC, Eby PR, Demartini WB, Gutierrez RL, Peacock S, Lehman CD (2011) Characterization of ductal carcinoma in situ on diffusion weighted breast MRI. Eur Radiol 21(9):2011–2019
7. Ernster VL, Ballard-Barbash R, Barlow WE, Zheng Y, Weaver DL, Cutter G, Yankaskas BC, Rosenberg R, Carney PA, Kerlikowske K, Taplin SH, Urban N, Geller BM (2002) Detection of ductal carcinoma in situ in women undergoing screening mammography. J Natl Cancer Inst 94(20):1546–1554
8. Yamada T, Mori N, Watanabe M, Kimijima I, Okumoto T, Seiji K, Takahashi S (2010) Radiologic-pathologic correlation of ductal carcinoma in situ. Radiographics 30(5):1183–1198
9. Kwee TC, van Ufford HM, Beek FJ, Takahara T, Uiterwaal CS, Bierings MB, Ludwig I, Fijnheer R, Nievelstein RA (2009) Whole-body MRI, including diffusion-weighted imaging, for the initial staging of malignant lymphoma: comparison to computed tomography. Invest Radiol 44(10):683–690
10. Heusner TA, Kuemmel S, Koeninger A, Hamami ME, Hahn S, Quinsten A, Bockisch A, Forsting M, Lauenstein T, Antoch G, Stahl A (2010) Diagnostic value of diffusion-weighted magnetic resonance imaging (DWI) compared to FDG PET/CT for whole-body breast cancer staging. Eur J Nucl Med Mol Imaging 37(6):1077–1086
11. Baltzer PA, Renz DM, Herrmann KH, Dietzel M, Krumbein I, Gajda M, Camara O, Reichenbach JR, Kaiser WA (2009) Diffusion-weighted imaging (DWI) in MR mammography (MRM): clinical comparison of echo planar imaging (EPI) and half-Fourier single-shot turbo spin echo (HASTE) diffusion techniques. Eur Radiol 19(7):1612–1620
12. Rahbar H, Partridge SC, Demartini WB, Gutierrez RL, Allison KH, Peacock S, Lehman CD (2012) In vivo assessment of ductal carcinoma in situ grade: a model incorporating dynamic contrast-enhanced and diffusion-weighted breast MR imaging parameters. Radiology 263(2):374–382
13. Basser PJ, Pierpaoli C (1996) Microstructural and physiological features of tissues elucidated by quantitative-diffusion-tensor MRI. J Magn Reson B 111(3):209–219
14. Tabar L, Tot T, Dean PB (2012) The basis for understanding the breast in health and disease, vol 1, 1st edn. László Tabár M.D, Sweden
15. Partridge SC, Murthy RS, Ziadloo A, White SW, Allison KH, Lehman CD (2010) Diffusion tensor magnetic resonance imaging of the normal breast. Magn Reson Imaging 28(3):320–328
16. Vashi R, Hooley R, Butler R, Geisel J, Philpotts L (2013) Breast imaging of the pregnant and lactating patient: physiologic changes and common benign entities. Am J Roentgenol 200(2):329–336
17. Partridge SC, McKinnon GC, Henry RG, Hylton NM (2001) Menstrual cycle variation of apparent diffusion coefficients measured in the normal breast using MRI. J Magn Reson Imaging 14(4):433–438
18. Baltzer PA, Schäfer A, Dietzel M, Grässel D, Gajda M, Camara O, Kaiser WA (2011) Diffusion tensor magnetic resonance imaging of the breast: a pilot study. Eur Radiol 21(1):1–10

19. Eyal E, Shapiro-Feinberg M, Furman-Haran E, Grobgeld D, Golan T, Itzchak Y, Catane R, Papa M, Degani H (2012) Parametric diffusion tensor imaging of the breast. Invest Radiol 47(5):284–291
20. O'Flynn EA, Morgan VA, Giles SL, deSouza NM (2012) Diffusion weighted imaging of the normal breast: reproducibility of apparent diffusion coefficient measurements and variation with menstrual cycle and menopausal status. Eur Radiol 22(7):1512–1518
21. Tabar L, Dean PB, Lindhe N, Ingvarsson M (2012) The ongoing revolution in breast imaging calls for a similar revolution in breast pathology. Int J Breast Cancer 2012:489345
22. Tabar L, Tot T, Dean PB (2005) Breast cancer: the art of science of early detection with mammography. Georg Thieme Verlag, Stuttgart
23. Muller-Schimpfle M, Ohmenhauser K, Stoll P, Dietz K, Claussen CD (1997) Menstrual cycle and age: influence on parenchymal contrast medium enhancement in MR imaging of the breast. Radiology 203(1):145–149
24. Kuhl CK, Bieling HB, Gieseke J, Kreft BP, Sommer T, Lutterbey G, Schild HH (1997) Healthy premenopausal breast parenchyma in dynamic contrast-enhanced MR imaging of the breast: normal contrast medium enhancement and cyclical-phase dependency. Radiology 203(1):137–144